Materials Today Bio 13 (2022) 100191

Contents lists available at ScienceDirect

Materials Today Bio

journal homepage: www.journals.elsevier.com/materials-today-bio

Broad virus inactivation using inorganic micro/nano-particulate materials

Sergio Rius-Rocabert [a,b,c], Javier Arranz-Herrero [a,b], Adolfo Fernández-Valdés [d], Marzia Marciello [e], Sandra Moreno [f], Francisco Llinares-Pinel [a], Jesus Presa [g], Rubén Hernandez-Alcoceba [h], Roberto López-Píriz [d], Ramón Torrecillas [d], Antonia García [c], Alejandro Brun [f], Marco Filice [e,i,j], José S. Moya [d], Belen Cabal [d,**], Estanislao Nistal-Villan [a,b,*]

[a] Microbiology Section, Dpto. CC, Farmacéuticas y de la Salud, Facultad de Farmacia, Universidad San Pablo-CEU, 28668, Madrid, Spain
[b] Facultad de Medicina, Instituto de Medicina Molecular Aplicada (IMMA), Universidad San Pablo-CEU, 28668, Madrid, Spain
[c] CEMBIO (Centre for Metabolomics and Bioanalysis), Facultad de Farmacia, Universidad San Pablo-CEU, 28668, Madrid, Spain
[d] Nanomaterials and Nanotechnology Research Center (CINN-CSIC), Universidad de Oviedo, Principado de Asturias, Avda de la Vega 4-6, El Entrego, 33940, Spain
[e] Nanobiotechnology for Life Sciences Group, Department of Chemistry in Pharmaceutical Sciences, Faculty of Pharmacy, Universidad Complutense de Madrid (UCM), Plaza Ramón y Cajal, 28040, Madrid, Spain
[f] Centro de Investigación en Sanidad Animal (CISA), Instituto Nacional de Investigación y Tecnología Agraria y Alimentaria - Centro Superior de Investigaciones Científicas (INIA-CSIC), Valdeolmos, Madrid, Spain
[g] Independent researcher
[h] Gene Therapy Program. University of Navarra-CIMA, Navarra Institute of Health Research, Av. Pio XII 55, 31008, Pamplona, Navarra, Spain
[i] CIBER de Enfermedades Respiratorias (CIBERES), Melchor Fernández Almagro, 3, 28029, Madrid, Spain
[j] Fundación Centro Nacional de Investigaciones Cardiovasculares Carlos III (CNIC), Melchor Fernandez Almagro, 3, 28029, Madrid, Spain

ARTICLE INFO

Keywords:
Virucidal materials
Virus inactivation
Virus clearance
Glass-based virucidal
Kaolinbased virucidal
Virus elimination

ABSTRACT

Inorganic materials can provide a set of tools to decontaminate solid, liquid or air containing viral particles. The use of disinfectants can be limited or not practical in scenarios where continuous cleaning is not feasible. Physicochemical differences between viruses raise the need for effective formulations for all kind of viruses. In the present work we describe two types of antimicrobial inorganic materials: i) a novel soda-lime glass (G3), and ii) kaolin containing metals nanoparticles (Ag or CuO), as materials to disable virus infectivity. Strong antiviral properties can be observed in G3 glass, and kaolin-containing nanoparticle materials showing a reduction of viral infectivity close to 99% in the first 10 min of contact of vesicular stomatitis virus (VSV). A potent virucidal activity is also present in G3 and kaolin containing Ag or CuO nanoparticles against all kinds of viruses tested, reducing more than 99% the amount of HSV-1, Adenovirus, VSV, Influenza virus and SARS-CoV-2 exposed to them. Virucidal properties could be explained by a direct interaction of materials with viruses as well as inactivation by the presence of virucidal elements in the material lixiviates. Kaolin-based materials guarantee a controlled release of active nanoparticles with antiviral activity. Current coronavirus crisis highlights the need for new strategies to remove viruses from contaminated areas. We propose these low-cost inorganic materials as useful disinfecting antivirals in the actual or future pandemic threats.

1. Introduction

Infectious diseases caused by viruses are one of the main global health concerns. The COVID-19 pandemic situation has been a challenge in many aspects, including the ability to decontaminate different materials [1]. Efficient pathogen removal from environments containing surfaces, liquids, or the air is challenging, due to the variability of scenarios, and the fact that the nature of microorganisms determines their half-live. In addition, viral infectivity can be determined by environmental factors such as composition, temperature, pH, humidity or redox properties [2–4]. Fomite-mediated virus transmission could be limited by the use of materials with virus disinfecting properties [5]. Viral disinfection has been a challenge since the discovery of viruses [6]. Virus characteristics may determine the need for cleaning viruses present in fomites [7], water or food in the case of viruses using the gastrointestinal entry route [8], or even airborne viruses [9]. Viruses that use the fecal-oral transmission

* Corresponding author. Microbiology Section, Dpto. CC, Farmacéuticas y de la Salud, Facultad de Farmacia, Universidad San Pablo-CEU, 28668, Madrid, Spain.
** Corresponding author.
E-mail addresses: b.cabal@cinn.es (B. Cabal), estanislao.nistalvillan@ceu.es (E. Nistal-Villan).

https://doi.org/10.1016/j.mtbio.2021.100191
Received 7 October 2021; Received in revised form 12 December 2021; Accepted 15 December 2021
Available online 22 December 2021

route can survive in sewage water and infect other hosts. Treatment of such waters may require specific disinfectants that do not alter water characteristics. Finally, airborne transmission and the presence of viruses both in droplets and aerosols generate important threats in situations such as the severe acute respiratory syndrome coronavirus 2 (SARS-CoV-2) pandemic or past Influenza virus outbreaks.

In view of the setbacks of antimicrobial organic materials such as low resistance to heat, high decomposability and short life span, new agents based on inorganic materials have been gaining a great research attention [10]. Within different materials already proposed for virus inactivation, nanomaterials represent a promising alternative. Metal-based nanoparticles show physicochemical properties related to high specific surface area and small size that allows the interaction with small infectious agents like viruses [11]. Many different metal and metal oxide nanoparticles such as silver, copper, zinc, gold, or titanium have been proposed as antiviral agents [12–17]. However, a known limitation of the practical application of nanoparticles is related with the possible environmental, health and safety (EHS) risks of nanoparticles. Thus, one possibility to overcome this limitation is to stabilize the nanosized materials in a clay matrix. Clay minerals are commonly used in the pharmaceutical industry as ingredients or additives [2,3]. Currently, they have been studied extensively as vectorized clays acting as advanced drug delivery systems for their potential biomedical applications [18]. They have large surface areas, adsorption capacity, large ion exchange capacity, thermal and chemical stability, excellent biocompatibility, low toxicity, and they are relatively abundant in nature which makes them a low-cost promising alternative in this field [3,19]. Chemical modification of clays such as intercalation of ions into the interlayer space of clay minerals or surface modification of clay mineral is a strategy to tune their properties for the loading and release of a drug [20,21]. For example, in a previous study by Cabal et al. [22] silver nanoparticles were successfully anchored on the surface of kaolin particles. Kaolin [$Al_2Si_2O_5(OH)_4$] is a plate-shaped, 1:1 clay mineral. Along with montmorillonite and sepiolite, kaolin is one of the most used clay minerals for the research and applications for medical purpose [23]. Kaolin particles act as a perfect nanoparticles dosing device allowing a controlled lixiviation of the metallic nanoparticles, keeping their concentration below the toxic limits for human cells and holding the bactericidal activity longer periods of time. Avoiding in this way agglomeration and health and environmental problems [22,24].

On the other hand, glasses and glass-ceramics are novel antimicrobial materials with a high potential in infection treatment. Most of the investigation carried out with these kinds of materials is with bioactive glasses and glass-ceramics. They are mainly used for bone repair and are being developed for tissue engineering applications. In recent years, there has been increasing interest in their potential antimicrobial properties. They have proven to be highly effective against some common clinically relevant pathogens, like *E. coli, P. aeruginosa, M. luteus, S. aureus*, including MRSA, *S. epidermidis, S. oralis, S. mutans, C. crusei, I. orientalis*, with no observed treatment resistance [25]. These types of materials also prevent bacterial growth [26], minimize bacterial adhesion, and prevent biofilm formation [27], even against multidrug-resistance (MDR) bacteria [28]; but their virucidal capacity has not been assessed so far. Various mechanisms have been proposed regarding their mode of action such as changes in the environmental pH and osmotic pressure or perturbations of the membrane potential of the microorganism [29]. These materials could provide an excellent substrate for engineering antimicrobial and other functional attributes against viruses to help expand the capabilities of these materials.

In this work, two different types of possible antiviral inorganic materials additives were prepared and evaluated; one is based on supported nanoparticles (i.e. silver or copper oxide) on a cationic clay (i.e. kaolin), and the other one is an antimicrobial glass. The effectivity of both material types was tested against model viruses such as non-enveloped viruses like adenovirus, or enveloped viruses such as vesicular stomatitis virus (VSV), influenza virus, pandemic coronaviruses SARS-CoV-2 as well as herpes simplex virus type I (HSV-1).

2. Materials and methods

2.1. Inorganic material analysis

2.1.1. Glasses

Two different glasses were tested against the viruses mentioned above. One is an antimicrobial glass powder, labeled as G3, with chemical composition (in mol.%): 40.3 SiO_2, 8.5 B_2O_3, 18.8 Na_2O, 19.2 CaO, 0.57 K_2O, 11.7 Al_2O_3 and 0.12 Fe_2O_3, obtained by the traditional melt-quench process, in a similar way as the one described by Moya et al. [12]. Briefly, the starting materials [oxides and carbonates of high purity (Merck KGaA, Darmstadt, Germany)] were mixed thoroughly and heated in platinum crucibles at 850 °C for 1 h to allow decarbonation. Subsequently, they were melted at 1400 °C for 1 h, and then quenched by dipping into water. The cooled glass frit was mill in a planetary ball milling using an agate high energy planetary ball mill grinding jar, and sieved to <50 μm, and the corresponding average particle size was found to be $d_{50} = 13$ μm. The other glass is a soda-lime glass, labeled as G1, with chemical composition (wt.%): 70.2 SiO_2, 1.1 B_2O_3, 15.8 Na_2O, 7.1 CaO, 0.05 K_2O, 1.7 Al_2O_3, 3.2 MgO, and 0.02 Fe_2O_3. This glass was also obtained by melt-quench method, fusing a mixture of the required stoichiometric amounts of the different oxides and carbonates of high purity (Merck KGaA, Darmstadt, Germany). The glass powder was also mill in a planetary ball milling and sieved to <50 μm ($d_{50} = 9$ μm). On contrary with G3 glass, G1 is not an antimicrobial glass [12]; In this work it was used as negative control. Glasses were storage at ambient temperature until the virucidal tests. A schematic representation of the process is shown in Fig. 1A.

2.2. Supported nanoparticles on kaolin

A commercial kaolin, supplied by CAVISA, La Coruña, Spain, was used. Its chemical composition (% w/w) is: 59.4 SiO_2, 33.1 Al_2O_3, 0.16 TiO_2, 0.40 Fe_2O_3, 0.24 CaO, 0.31 K_2O, 6.16 LOI, 0.23 others. Supported nanoparticles on kaolin were obtained following a chemical reduction route similar as the one described by Cabal et al. [7]. $AgNO_3$ and $Cu(NO_3)_2$ (supplied Merck KGaA, Darmstadt, Germany) were used as precursor of silver and copper oxide, respectively. The content of silver and copper oxide nanoparticles in kaolin was 2% and 5% respectively. Supported nanoparticles on kaolin powders were sieved to <50 μm. The average kaolin particle size is $d_{50} = 9$ μm. The unmodified kaolin sample was labeled as K, and modified kaolin with silver or copper oxides nanoparticles were labeled as K-nAg and K-nCu, respectively. Kaolin based materials were storage at ambient temperature until the virucidal tests. A schematic representation of the process is shown in Fig. 1B.

2.3. Characterization of inorganic antimicrobial materials

The mineralogical composition of the samples was determined by X-ray diffraction (XRD) using a Bruker D8 Advance diffractometer (Billerica, Masshachuttet, USA) with CuKα radiation at 40 kV and 30 mA in a step-scanning mode from 4° to 70° with a step width of 0.05° and a step time of 0.5 s. Particle size analysis was performed in a Beckman Coulter LS Particle Size Analyzer. The specific surface areas were calculated using the BET method from the N_2 adsorption isotherms within the relative pressure (p/p°) range 0–0.27. N2 isotherms at −196 °C were recorded using a Micromeritics ASAP 2420.

2.4. Cells

Vero (VERO C1008, Cat#CRL-1586™, Manassas, VA, USA), HEK293T (ATCC® CRL-3216™, Manassas, VA, USA), Huh7.0 (ATCC® PTA-4583™, Manassas, VA, USA), MDCK-NS1 (provided by Adolfo García-Sastre laboratory at Mount Sinai) were cultured in Dulbecco's

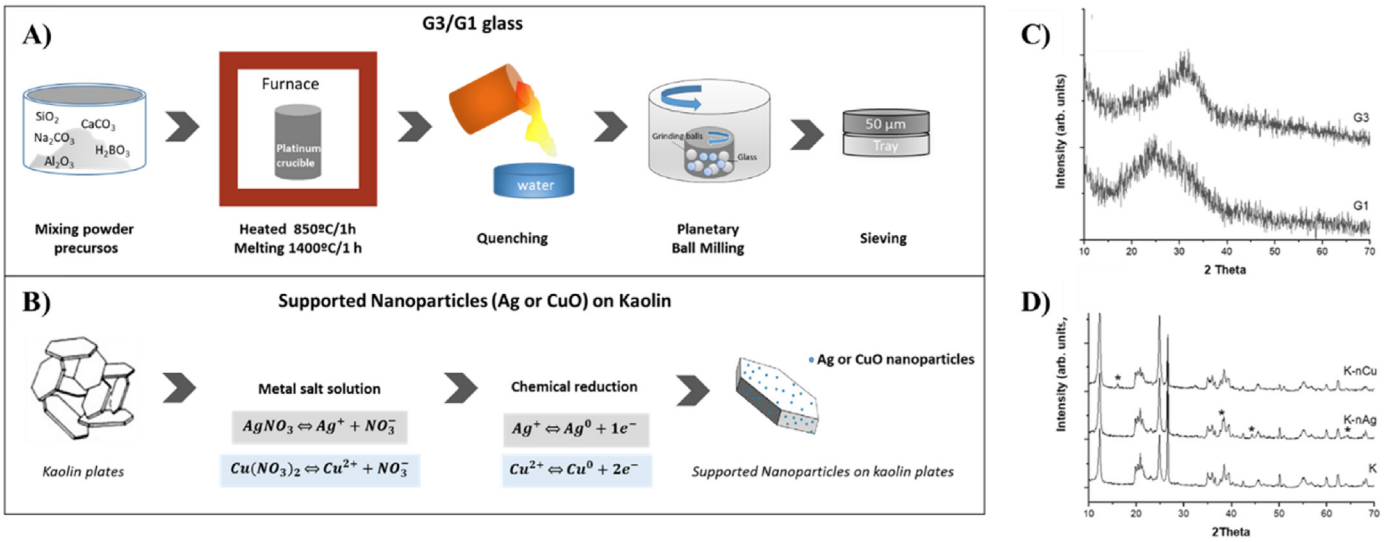

Fig. 1. Characteristics of the materials: A) The preparation of G3 or G1 glass and **B)** supported nanoparticles (Ag or CuO) on kaolin. **C)** XRD patterns of G1 and G3 glasses, and **D)** kaolin (K), supported silver nanoparticles on kaolin (K-nAg), and supported copper oxide nanoparticles on kaolin (K-nCu). Peaks ascribed to metallic silver and to copper oxide are identified with an asterisk.

Modified Eagle Medium (DMEM) (Gibco™, Waltham, MA, USA) supplemented with 10% of fetal bovine serum (FBS) (Gibco™, Waltham, MA, USA) and 1% of penicillin/streptomycin (Gibco™, Waltham, MA, USA) (referred as complete DMEM) and maintained in an incubator at 37 °C with 5% of CO_2 and 90% humidity. SIRC (ATCC® CCL-60™, Manassas, VA, USA) cells were grown as described previously for growing HSV [30].

2.5. Cell viability assays

96-well plates were used to plate 10,000 Vero cells/well in 100 µl. In parallel, 500 µl of each material were incubated in triplicates with 1 ml of complete DMEM media for 24 h in slow rotatory movement at 25 °C. One day later, cells were incubated with serial dilutions of the supernatants or DMEM media (control), and 24 h later, cell viability was assessed by using the MTS reagent (Promega, Madison, WI, USA) following manufacturer indications. Absorbance was recorded at 490 nm and 630 nm using a Varioskan Lux (Thermo Fisher Scientific, Waltham, MA, USA) spectrophotometer plate reader. Values were calculated in reference to the viability of mock-infected cells (negative control). Cell viability (%) = [Absorbance infected-sample/Absorbance mock-infected sample] × 100. Mock-infected samples refers to DMEM media without virus.

2.6. Viruses

2.6.1. Virus growth and maintenance

Recombinant VSV-GFP was grown in Vero cells by 0.001 Multiplicity of Infection (MOI) infection for 48 h [31]. Stocks were rapidly frozen in dry ice and maintained at −80 °C. Stock titration was performed by direct fluorescence measurement after 48 h of Vero cells infection. Tissue culture infection dose 50 (TCID50) was calculated by the Reed-Muënch method [33]. Recombinant adenovirus serotype 5 with insertion of GFP in the E3 region (Ad5-GFP) was produced as previously described [32]. The HSV-1 encoding GFP (HSV-1 Cgal + IGR20-EGFP), referred hereinafter to as HSV-1-GFP [30] was grown in rabbit Sirc cells infected at an MOI of 0.01. SARS-CoV 2 was grown for 3 days in clonal Vero E6 (ATCC-CRL/1586) cells infected at an MOI of 0.01. Stocks were rapidly frozen in dry ice and maintained at −80 °C. Stock titration was performed by plaque assay.

Influenza virus was grown for two days in 9 days old chicken embryonated eggs infected with 500 plaque forming units (pfu). Specific-Pathogen-Free (SPF) chicken embryonated eggs were donated by Granja Rodríguez Serrano in Alba de Tormes, Salamanca, Spain. Two days after inoculation, allantoid liquid was recovered, centrifuged, aliquoted and quickly frozen in dry ice. Virus titers were determined in MDCK-NS1 cells.

2.6.2. Analysis of virus inactivation in suspension

One million viral infective particles diluted in 500 µl of complete DMEM culture medium wereadded to a volume of 500 µl of previously sterilized powdered material or 500 µl media (negative control) and incubated in 2 ml centrifuge tubes under a 10-rpm rotational movement at 25 °C during the indicated times. Incubation was followed by addition of 500 µl of media, vortexing and centrifugation of the tubes at 7000 G for 5 min at room temperature to achieve separation of the viral solution from the solid material. Supernatant was collected in new tubes. A second centrifugation was carried out to eliminate possible remains of the solid material. Serial dilutions of the supernatants were made to titrate the viruses under study in the appropriate cell lines.

2.7. Statistical analysis

Statistical analysis was performed using a 2-tailed Student *t*-test and one way and two-way ANOVA followed by Bonferroni and Kluskal-Wallis post-tests. Data are presented as means ± standard deviation and were calculated using the software package GraphPad Prism v. 5.0. (GraphPad Software, San Diego, CA, USA). Statistical values of $p < 0.05$ were considered significant.

2.8. Study of the mechanism of action

2.8.1. Inductively coupled plasma spectrometry (ICP)

To determine the presence of each element in the lixiviates in contact with the different materials, inductively coupled plasma spectrometry (ICP) was carried out. Eppendorf tubes were filled with each material up to the 500 µl mark and incubated with 1 ml of complete DMEM for 1 h. The supernatant was then separated by two sequential centrifugations for 5 min at 14,000 rpm in an Eppendorf centrifuge and kept at −80 °C till

thaw at the moment of analysis. Each supernatant was diluted 1/25 in 1% HNO_3 in milliQ H_20 and then analyzed with any further dilution, diluted 1/10 and 1/100 and analyzed in triplicate using inductively coupled plasma-optical emission spectrometry (ICP-OES). The experiment was performed with an Agilent Varian ICP-OES (Santa Clara, CA, USA).

The amount of silver and copper released into supernatant from K-nAg and K-nCu, respectively, was determined for different time intervals up to 24 h. Eppendorf tubes were filled with 0.23 g of K-nAg and 0.32 g of K-nCu. Each material was incubated in 1.5 ml of complete DMEM under a 10-rpm rotational movement at 25 °C. At defined time intervals of 10 min, 30 min, 8 and 24 h, the supernatant was then separated by two sequential centrifugation for 5 min at 14,000 rpm in an Eppendorf centrifuge. The released silver and copper was measured by inductively coupled plasma-mass spectrometry (ICP-MS) (ICP-MS Agilent 7700x, Santa Clara, CA, USA).

2.9. Transmission electron microscopy (TEM)

Particle size and shape were studied by transmission electron microscopy (TEM) using a JEOL-2000FXII microscope (JEOL Ltd., Tokyo, Japan) operating at 200 keV. TEM samples were prepared by placing one drop of a dilute suspension of inorganic materials in milli Q water on a carbon coated copper grid and allowing the solvent to evaporate slowly at room temperature. The mean particle size (DTEM) and distribution were evaluated by measuring at least 200 particles and fitting the data to a log normal distribution. For the highest resolution images, a 200 keV Philips Tecnai 20 microscope was used.

2.10. Western blot

Proteins were separated by SDS-PAGE (Bio-Rad, Hercules, CA, USA) and then transferred onto polyvinylidene difluoride membranes (Millipore, Burlington, MA, USA) following the manufacturer's instructions. After blocking with 5% milk, the membranes were incubated with an anti VSV-G-tag antibody (Genstript Biotech, Piscataway, NJ, USA) at 1:500 dilution. After being washed with phosphate-buffered saline containing 0.5% Tween 20, the membranes were incubated with a horseradish peroxidase-conjugated anti-rabbit immunoglobulin secondary antibody (Cell Signaling Technology, Danvers, MA, USA). The horseradish peroxidase immunocomplexes were detected using an enhanced chemiluminescence kit (Alkali Scientific, Pompano Beach, FL, USA) in a ChemiDoc imaging system (Bio-Rad, Hercules, CA, USA).

2.11. Protein quantification

The quantification of proteins in the different materials was performed by using the Micro BCA protein assays kit (Thermo Scientific, Waltham, MA, USA) following manufacturer instructions. Briefly, supernatants or materials in contact with viruses were incubated with 500 μl of BCA at 60 °C for 1 h. Protein presence was quantified tree times in reagent-containing supernatants by measuring absorbance at 562 nm in a Varioskan Lux (Thermo Scientific, Waltham, MA, USA) plate reader.

2.12. Dynamic light scattering (DLS)

Hydrodynamic diameter and surface ζ-potential measurements were acquired on a Dynamic Light Scattering (DLS) Zetasizer Nano Zen 3600 (Malvern Panalytical Ltd, Malvern, UK), diluting samples in potassium nitrate aqueous solution (KNO_3, 0.01 M). The hydrodynamic size of the particles in suspension was measured by DLS in intensity mode diluting the sample in ultrapure water and the electrophoretic mobility was measured as a function of pH at 25 °C, using 10−2 M KNO_3 as electrolyte and HNO_3 and KOH to change the pH of the suspensions. Each hydrodynamic value is the result of three different measurements at different dilutions to avoid errors coming from backscattering.

3. Results

3.1. Characterization of the inorganic materials

G3 and G1 powders were prepared by glass powder manufacturing method (i.e., melting and quenching processes) starting from carbonates and oxides (Fig. 1A). In the case of supported nanoparticles (Ag or CuO) on kaolin, a chemical reduction approach was followed. The method is based on the chemical reduction in aqueous silver/copper salt using sodium borohydride as reducing agent (Fig. 1B). The characteristics of the materials under analysis were initially characterized by X-ray diffraction. The patterns of glass samples (Fig. 1C) did not reveal sharp peaks, broad humps characteristic of amorphous materials are clearly visible. In the case of the supported nanoparticles in kaolin (Fig. 1D), mineral identification was confirmed by XRD. Kaolinite (PDF 78–2110) and quartz (PDF 65–0466) were recognized as the constituents of the used kaolin. Comparing the XRD patterns, K-nAg exhibits new peaks at 38.2°, 44.4° and 64.5° that can be ascribed to metallic silver (PDF 87–0717), and in the case of K-nCu a new peak at 16.15° can be ascribed to CuO (PDF 44–0706).

3.2. Antiviral activity against vesicular stomatitis virus (VSV)

Antiviral activity of the materials under study was initially tested using vesicular stomatitis virus (VSV) as a model. The virus was incubated with DMEM media alone or media together with each material with a constant rotatory movement in a stove at 25 °C for 10 min, 30 min or 8 h. The virus recovered from the liquid phase was then titrated. As reported in Fig. 2, kaolin-based materials present an intense ability to reduce the virus amount remaining in the supernatant even after 10 min of incubation. Shorter times were not feasible due to sample processing times. A significant decrease in the virus present in the supernatant was also observed in the G3 glass-based materials, however, in this case, the G3 glass material presented a significant effect of VSV as soon as 10 min, and a complete disappearance of the virus from the liquid phase after 8 h of incubation. Exact values for means and ±SD are listed in Supplementary Table 1.

3.2.1. Cytotoxicity

The absence of virus in the media in contact with the material could be the indirect effect of the material substances on cell viability. To address this possibility, toxicity of substances potentially released into the media was determined by using the MTS cell viability assay. Twenty-four hours after incubation with the solid materials, the liquid media was separated by centrifugation and serially diluted before it was exposed to Vero cells. The presence of toxic substances for Vero cells in lixiviates coming from the different materials incubated for 24 h with the different materials showing activity against VSV can be observed in Fig. 3. DMEM alone was used as negative control.

Control media and the corresponding dilutions sets of each material were evaluated by the MTS reduction. The materials showed mild to moderate toxicity. G3 glass secretes toxic factors into the media that reduce around 50% cell viability using 1/3 dilution of the media supernatant in contact with the material supernatant. K-nCu presented the highest toxicity, where even a 1/9 dilution of the preconditioned media presents high toxicity on Vero cells. In comparison, K-nAg had little effect on cell activity, comparable to the control media. Exact values for means and ±SD are listed in Supplementary Table 2.

3.2.2. Mechanism of action

To determine the possible mechanisms behind VSV disappearance, we first studied the ability of material lixiviates to have any antiviral activity. Supernatants in contact with 500 μl of the different materials were exposed to a fixed amount of VSV-GFP (10^6 infective particles). The materials were incubated with the media for 24 h followed by an incubation of a constant amount of virus for 1 h. In Fig. 4A, we can appreciate

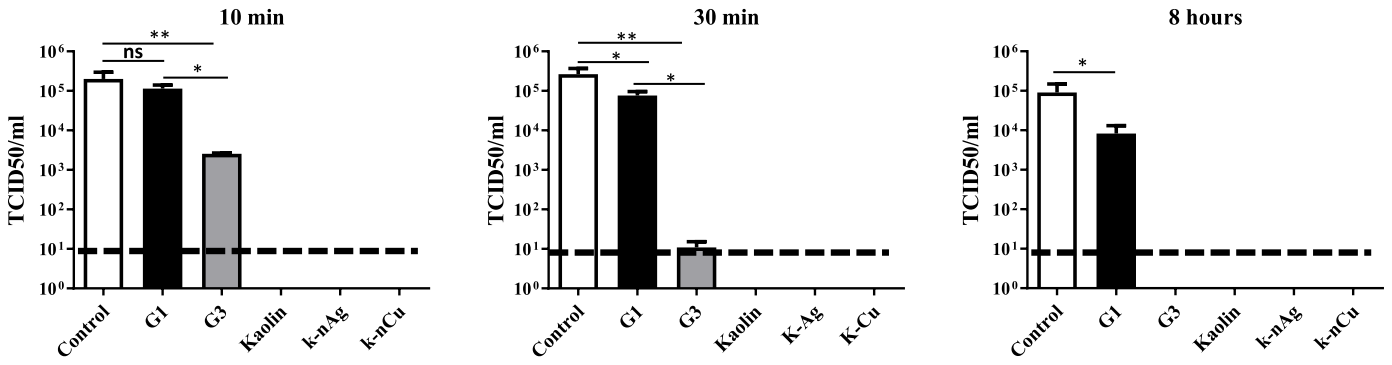

Fig. 2. Time course of the antiviral activity of inorganic materials. TCID50 values of remaining VSV-GFP from 2 × 10^5 TCID50 VSV-GFP/ml incubated with indicated materials for 10 min, 30 min or 8 h. Virus present in the supernatant was titrated in Vero cells using the Reed-Muench method. Dotted lines represent the limit of the detection by the assay. One way ANOVA followed by Bonferroni post-test was used to determine statistical differences. ***: $p < 0.001$; **: $p < 0.01$; *: $p < 0.05$; ns: not significate. N = 3. Error bars correspond to ±SD.

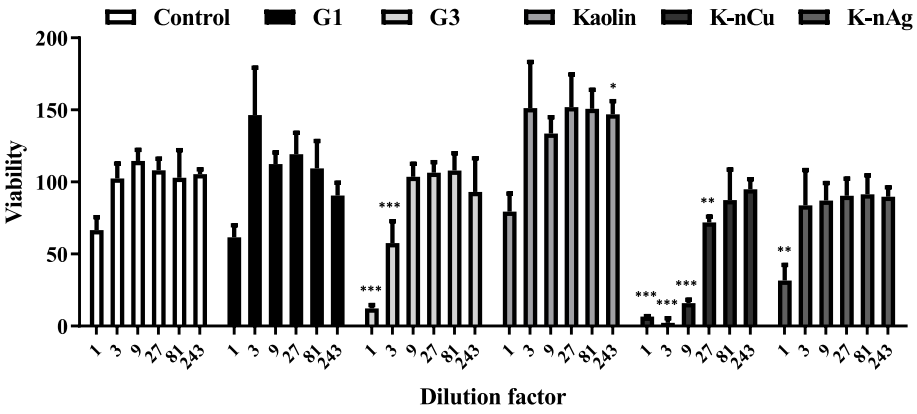

Fig. 3. Toxicity of substances released into cell media in contact with materials under study. Supernatant to determine cell viability was obtained by incubating complete DMEM media alone (control) or with 500 μl of the different materials in rotatory movement at 25 °C for 24 h. Cell viability assay was determined using the MTS assay on Vero cells exposed to serial dilutions of the incubated media. One way ANOVA followed by Bonferroni posttest was used to determine statistical differences. ***: $p < 0.001$; **: $p < 0.01$; *: $p < 0.05$; ns: not significate N = 3. Error bars correspond to ±SD.

that there is a significant decrease in the viable VSV exposed to the K-nCu lixiviate as well as a lower effect of lixiviates coming from G3 and K-nAg. Exact values for means and ±SD are listed in Supplementary Table 3.

Determination of the inhibitory concentration in lixiviates was performed by mixing VSV with 1/2, 1/5 or 1/10 lixiviate dilutions. In Fig. 4B 1/2 dilutions still retain inhibitory power, which seems to disappear at 1/5 in the case of G3 and K-nAg. At 1/10 dilution, some inhibitory effect seems to be retained by K-nCu. Extended incubation of lixiviates with VSV for 24 h was analyzed as well. In Fig. 4C, it can be appreciated the virus inactivation properties of the G3, K-nCu and K-nAg, showing a reduction between 3 and 4 orders of magnitude the remaining virus in contact with lixiviates in comparison with the control.

Based on the results obtained with the incubation of lixiviates with the virus for 1 h, in Fig. 4D left panel we can appreciate the percentage of virus inactivation as compared to the control for each of the dilutions performed. A projection of those results was performed in Fig. 4D right panel. In order compare the inhibitory power of the different materials, the 90% of inhibitory power of K-nCu was set as a reference. In this panel we can observe the dilution of each lixiviate required to inhibit 90%, 95% or 99% of the initial amount of VSV for G3, K-nCu and K-nAg.

The properties of lixiviates prompted to better describe the composition of some of the differential elements present in the materials. In Fig. 4E, the amount in mg/l of sodium (Na), copper (Cu), silver (Ag), and aluminum (Al) was analyzed with the help of an ICP-OES spectrometer. There is a clear release of these elements into the DMEM media represented as Ctr. Specifically, G3 can liberate Al ions, while K-nCu can release Al ions in addition to Cu ions. K–Ag nanoparticles can liberate Al ions in addition to Ag ions.

Attending to the inhibitory effect of materials against VSV observed in Figs. 2 and 4, it seems the antiviral properties cannot be explained exclusively by the substances present in the lixiviate of the materials under analysis. Additional virus inhibition could be explained by direct virus-material contact, including the adsorption of the virus by the material. To visualize whether some virus may be transferred from the material to the cells, the different materials incubated with VSV were washed three times by adding 1 ml of 1X PBS, mixing by vortexing, centrifuging, and removing the PBS to later expose Vero cells to them for 1 h. In this case, the positive control was not material, but a virus containing supernatant. After that, the material was removed, and cells washed with 1X PBS to prevent toxic effects. As observed in Fig. 5A, 24 h after incubation, GFP expression from VSV-GFP infected cells could be observed in cells in contact with G1, G3, Kaolin, but not in cells in contact with K-nCu and K-nAg. Cells incubated with K-nCu and K-nAg were still viable and appeared similar to the control untreated Vero cells (Supplementary Fig. 1). Together with bright field images, UV images showed presence of recombinant viral codified GFP, implying the active protein expression of viable cells. In the case of K-nCu and K-nAg viral GFP cannot be observed, but cell morphology indicates the presence of attached viable cells.

3.2.3. *Characterization by transmission electron microscopy (TEM)*

Further visual exploration of K-nCu and K-nAg materials under study was performed by transmission electron microscopy (TEM). After 1 h of incubation of 500 μl of the material with 10^6 VSV-GFP infective particles, material was recovered, and a small fraction (one drop) of it was prepared to be observed by TEM (Fig. 5B). Observations of starting kaolin-based particles show the classical polyhedral-shaped platelets. TEM images also provide evidence of the quite homogeneous distribution of silver and copper oxide nanoparticles on the kaolin plates. Accumulation of high-density metal containing nanoparticles could be observed outside

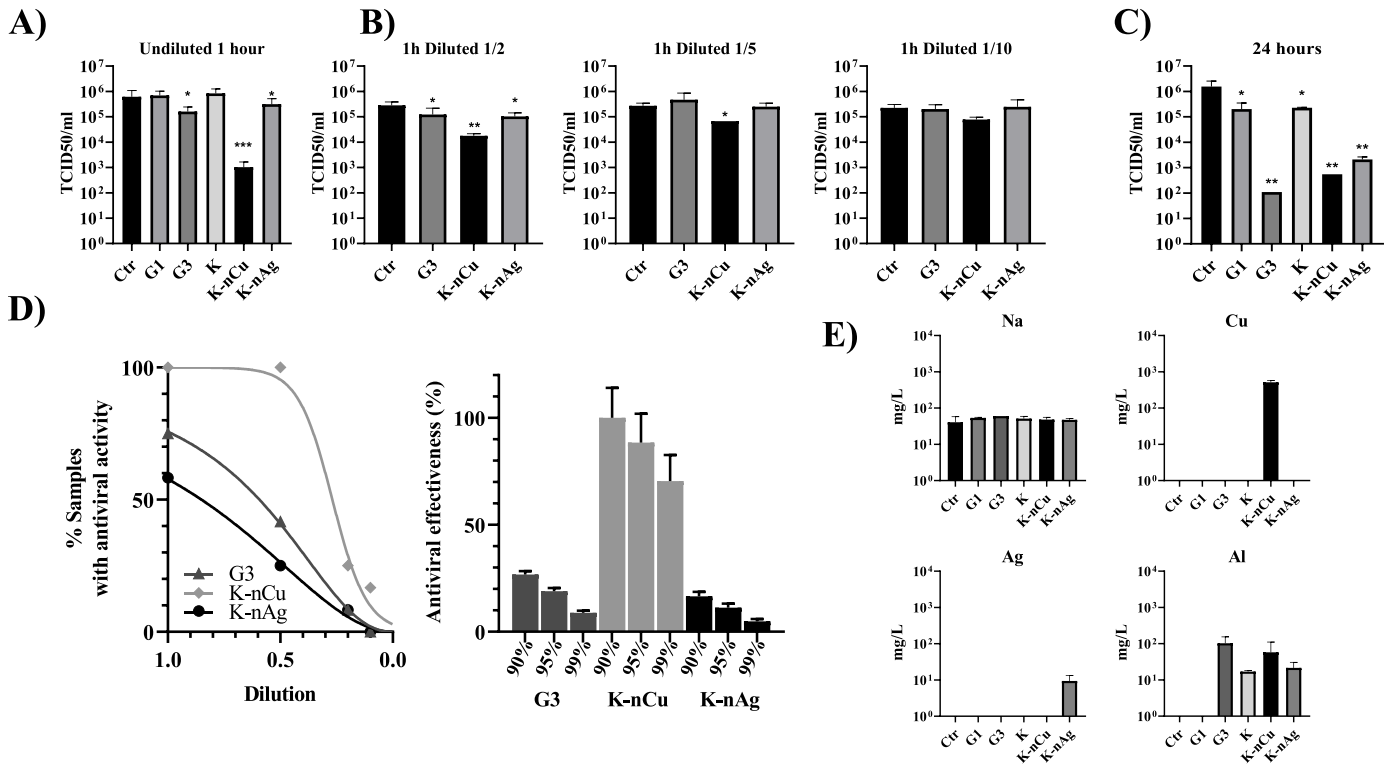

Fig. 4. Antiviral properties of lixiviates in contact with the different materials under study. A) 24 h after the incubation of 500 μl of the different materials with 1 ml of complete DMEM median, lixiviates were incubated with 10^6 VSV-GFP infective particles. TCID50/ml represents the viable virus remaining after 1 h of incubation with these conditionate media. **B)** 1/2, 1/5 and 1/10 serial dilutions of the lixiviate form samples showing some inhibitory activities were analyzed to determine their TCID50 against VSV-GFP. **C)** As in A) but virus was incubated with lixiviates for 24 h. **D)** Left: Graph represents the percentage of G3(▲), Cu(◆), and Ag(●) samples that show antiviral ability versus their dilution value at 1 h of incubation. The 0.05% of the control is taken as the cutoff value, below which a sample is considered to have anti-viral activity. Right: projection of the inhibitory potential of each lixiviate. The fit to the experimental points was made based on a 4-parameter logistic model forcing the parameter corresponding to the Lower Value to zero. **E)** ICP analysis of elements present in lixiviates from A). Kluskal-Wallis test was used to determine statistical differences. ***: $p < 0.001$; **: $p < 0.01$; *: $p < 0.05$; ns: not significate. N = 3. Error bars correspond to ±SD.

of the particles (lower panels). Interestingly, some of these nanoparticles were aggregated together with some low-density material different from the kaolin particles that may come from the media containing viruses. This observation is coincidental with the presence of some of elements described in Fig. 4E that can explain the destruction of virus particles.

3.2.4. Determination of released silver and copper

The release rate of silver and copper from kaolin-based materials was evaluated by inductively coupled plasma-mass spectrometry (ICP-MS). The cumulative concentration of silver and copper was obtained and plotted versus time (Fig. 5C). The levels of silver leached from kaolin-nAg was ~2.4 ppm in the first 10 min. No significant increase was detected 30 min and 8 h later. 24 h later the content of released silver increased only 0.6 ppm with respect with the quantity of released silver in the first 10 min. The levels of copper leached from kaolin-nCu was ~247 ppm in the first 10 min. Similar trend to silver was observed for copper at higher times. 24 h later the content of released copper increased only 0.3 ppm with respect with the quantity in the first 10 min.

3.2.5. Protein quantification

To better characterize the possible mechanisms behind the ability of the different materials to remove viruses from the solution, the amount of total protein present in the supernatant in contact with the materials was determined by Bradford protein assay. VSV was incubated with 500 μl of the different materials for 1 h. After separation of the liquid phase from the material by centrifugation, total protein remaining in the liquid phase was determined. As observed in Fig. 6A, the protein quantification in the supernatant in contact with G1 and G3 glasses was equivalent as compared to the original initial protein amount present in the virus preparation. In comparison, the amount of total protein present in the supernatants in contact with the kaolin-based materials is less abundant and in the case of the materials containing CuO and Ag, the amount of protein remaining was residual. Exact values for means and ±SD values are listed in Supplementary Table 4.

A fraction of the supernatant and a protein extraction using 10% SDS was mixed to load and run a PAGE and transfer the proteins into a PVDF membrane. In panels Fig. 6B and 6C a Ponceau staining of the proteins transferred into the membrane shows a clear band corresponding to the molecular weight of the VSV G protein in the liquid phase of Control, G1 and G3 (Fig. 6B). In the case of the kaolin-based materials however, only the VSV-G band can be visualized using Ponceau technique (Fig. 6C).

To try to understand the disappearance of these proteins, a Western blot was performed on the same membrane using a polyclonal antibody that detects the YTDIEMNRLGK peptide present in the VSV G protein. Surprisingly, the detection of the proteins by WB in G1 and G3 (Fig. 6D), is different than the one observed in Fig. 6B, showing a drastic reduction of VSV G. In addition, protein detection by WB allows the visualization of discrete higher molecular weight stable protein S species, that can be better observed in the G3 condition.

Fig. 6E shows the WB of the samples incubated with the kaolin-based materials. In this case, in addition to determine the presence of VSV-G in the media, we include samples containing proteins extracted from the material by using SDS. No protein could be observed in any of the supernatants, however, some protein can be detected associated to the material, after SDS and boiling extraction. Different protein extraction methods were used to try to extract the proteins from the kaolin-based materials, including pH, high electricity voltage of high salt concentration. None of them was able to efficiently extract the proteins from the

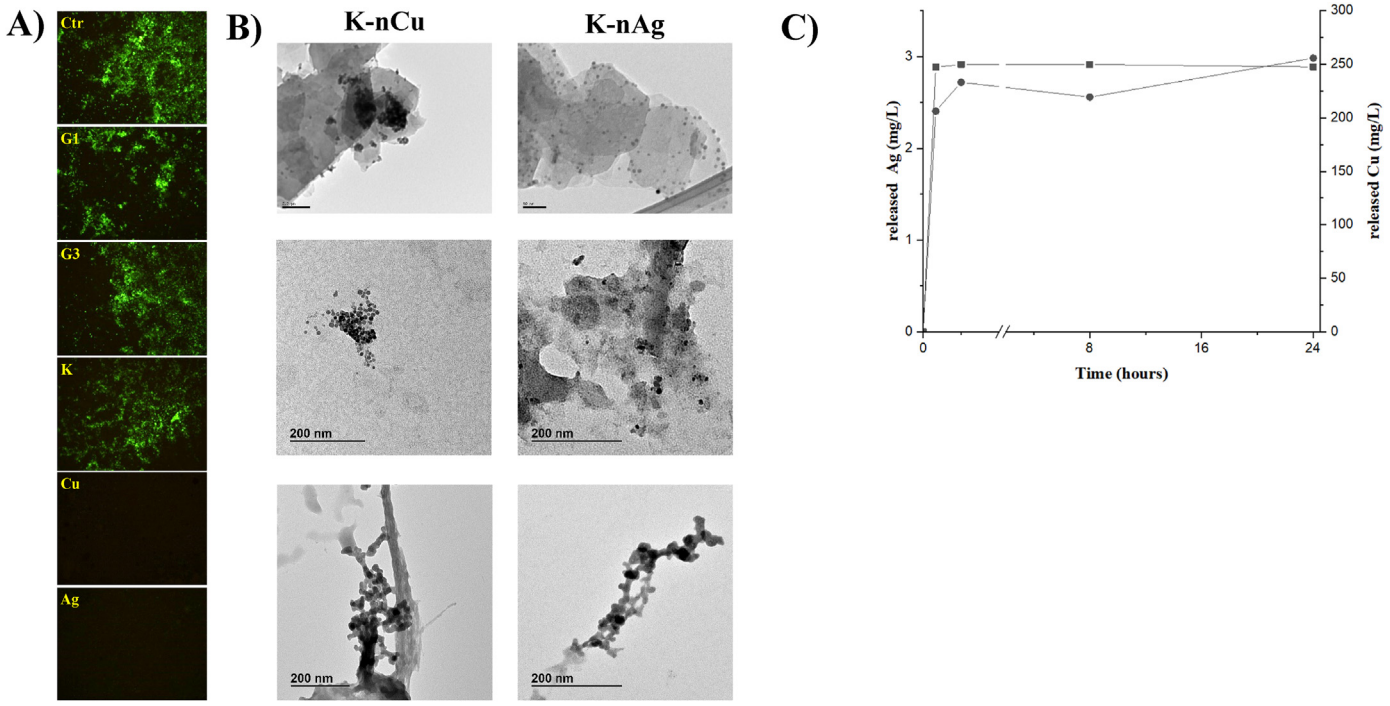

Fig. 5. Virucidal activity directly present in the materials. A) GFP expression in Vero cells incubated for 1 h with 10^6 VSV-GFP in DMEM media (positive control) or 500 μl of the different materials previously incubated with 10^6 VSV-GFP viral particles and washed 3 times with 1X PBS. **B)** TEM micrographs showing the characteristic of the K-nCu and K-nAg materials being incubated with VSV. Top: Image of the materials under study (scale 50 nm). Bottom: selected images showing the accumulation of metal-base NP released from the material. **C)** ICP-MS values Cumulative silver released (■) from K-nAg and copper released (●) from K-nCu in complete DMEM media at 25 °C as a function of time.

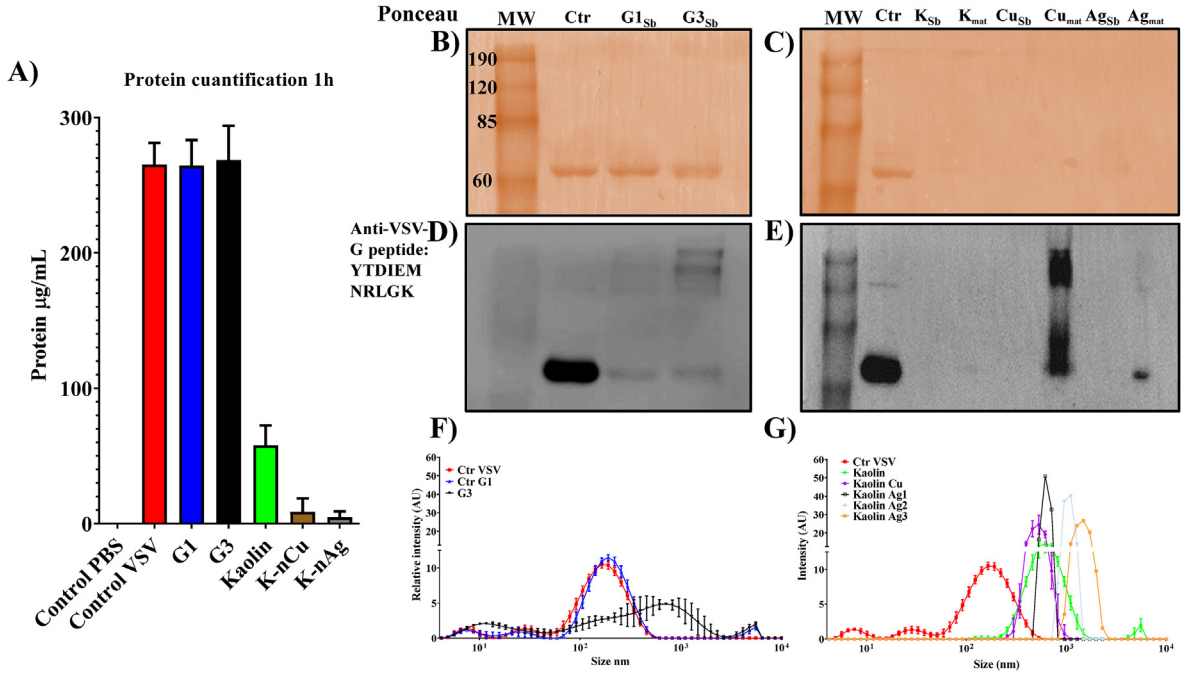

Fig. 6. Effects of materials on VSV viral proteins. A) Bradford protein quantification of VSV containing supernatants in contact with the different materials under study. **B)** and **C)** Ponceau S staining of PVDF membranes. VSV containing supernatants (Sn) in contact with the different materials and the materials themself (Mat) were diluted with Laemmli buffer 2X and run in a 10% SDS-PAGE gel and proteins were transferred into PVDF membranes before staining. In B) the G1 and G3 samples in comparison with the Ctr. In C) the kaolin-based samples. **D)-E)** WB of the same membranes using a polyclonal Ab against YTDIEMNRLGK peptide present in VSV-G. D) Correspond to B) samples and E) corresponds to C) samples. **F)-G)** Dynamic light scattering analysis of VSV containing supernatants that were exposed F) to G1 and G3 and G) to the kaolin-based materials. N = 3. Error bars correspond to ±SD.

material, suggesting a tight binding of these materials to the virus.

3.2.6. Characterization by dynamic light scattering (DLS)

To further characterize the effect of the different materials on the virus, the VSV supernatants in contact with the different materials were analyzed by dynamic light scattering (DLS). This technique allows the detection of different particles in solution by determining their size. In Fig. 6F we can observe that the virus incubated with G1 marginally modifies the size as compared to the control virus, however, G3 has a profound effect, altering the average size of the particles and generating species of higher molecular weight. When DLS is used to determine the effect of the kaolin-based materials on VSV (Fig. 6E), we can observe an overall increase of particle size in supernatants from the kaolin control, as well as the one containing CuO nanoparticles. The species present in the supernatant of the kaolin material containing Ag were highly variable. Individual samples are presented instead of the average values to visualize the heterogeneity of individual measurements.

It is important to notice that the Y axis represents arbitrary units of intensity, which cannot be used to determine and compare the number of particles in each of the samples when the number of particles is different between them. In this sense, the total intensity particles present in Fig. 6F could be compared but not in Fig. 6G, were almost no protein was detected in supernatants. Analysis of ζ-potential in materials incubated with VSV was also performed to determine a change of charge in the materials in contact with the virus (Supplementary Table 5). A marked potential decrease in glass-based materials incubated with VSV was observed. In the case of Kaolin, ζ-potential reduction is observed as well, however in the kaolin-based nanoparticles containing Cu or Ag, the ζ potential is increased in the case of K-nCu and marginally decreases in the case of K-nAg.

3.2.7. Antiviral activity against adenovirus 5, HSV-1, influenza virus, and SARS-CoV-2

In experiments performed so far, VSV virus has been used as the only model to determine antiviral properties of the different materials. To further determine the antiviral properties of inorganic powder-based materials on human relevant viruses, we choose a set of viruses with different characteristics. Adenovirus is a model of non-enveloped viruses causing respiratory, ocular, and gastrointestinal infections. In Fig. 7A, we can appreciate that after 1 h of incubation with the virus, G3 and the K-nCu materials present a complete dissapearance in the amount of virus presented in the supernatant in contact with the material. In addition, incubation with K-nAg had the ability to reduce around 1000 times the virus infectivity. Both G1 and the kaolin controls had also some residual activity, reducing around 10 times the amount of adenovirus remaining in the supernatant.

HSV-1 can be considered a model of enveloped virus with internal icosahedral capsid that presents important human burden causing skin

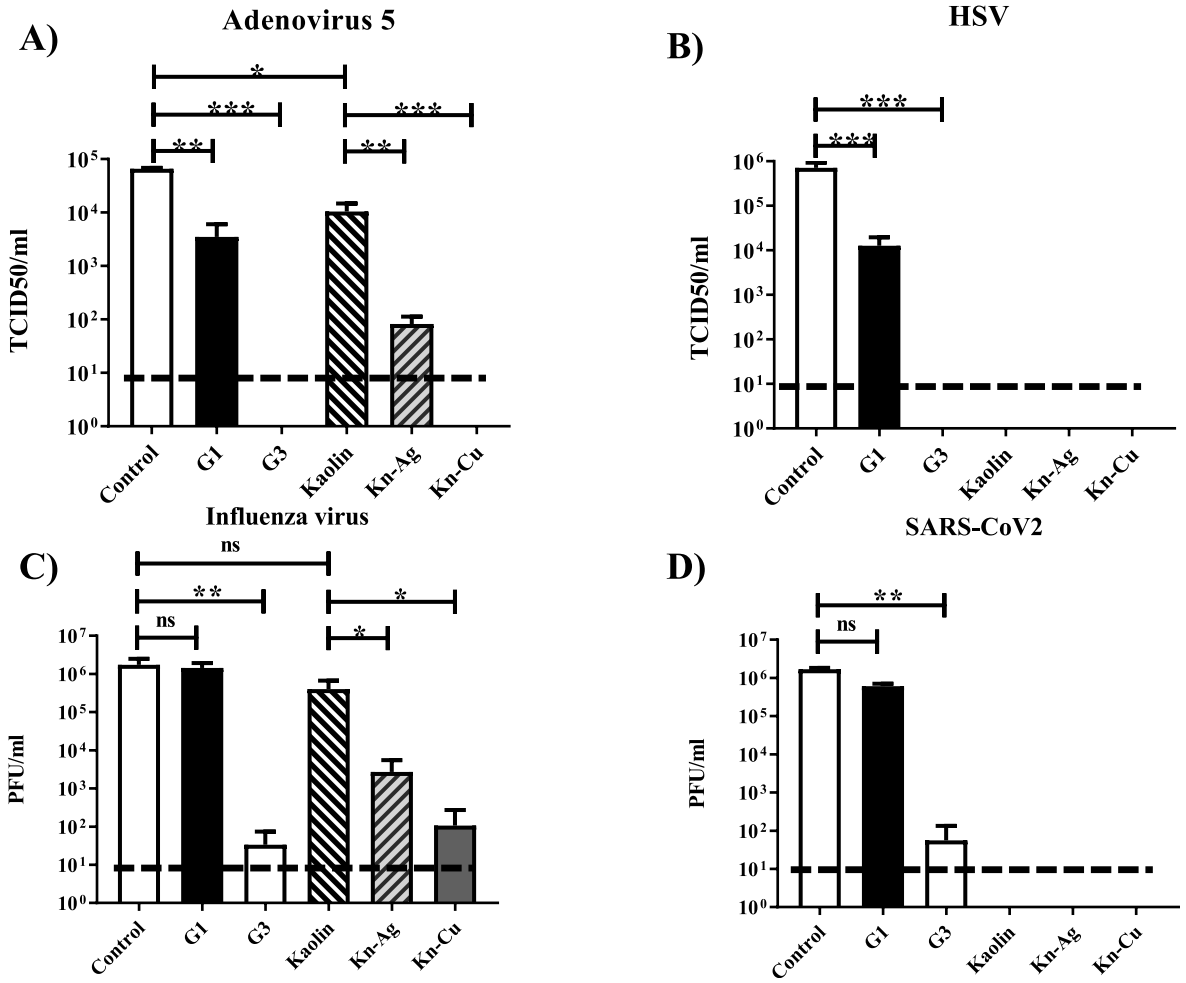

Fig. 7. Antiviral activity of the inorganic materials on human relevant viruses. The ability of materials to reduce the virus present in the supernatants containing **A)** Adenovirus 5-GFP, **B)** HSV-1-GFP, **C)** Influenza virus A/PR/8/34 or **D)** SARS-CoV-2 is analyzed by incubating the materials in the form of powder together with the individual viruses in rotatory movement at 25 °C for 1 h. The virus remaining in the supernatant was titrated in Vero cells for Adenovirus 5-GFP, HSV-1-GFP and SARS-CoV-2. Influenza virus was titrated in MDCK-NS1 cells. Dotted line represents the limit of the detection by the assay. ***: $p < 0.001$; **: $p < 0.01$; *: $p < 0.05$; ns: not significative. N = 3. Error bars correspond to ±SD.

and neuronal infections. The effect of the materials in this virus was analyzed in Fig. 7B. We used an HSV-1-GFP that allows a quick determination of viral titers. In this case, G1 presented a reduction of the viable virus remaining in the supernatant close to 100 times. G3 and all the kaolin-based materials were able to completely remove HSV-1 from the supernatant in contact with the material.

Influenza virus is an enveloped virus causing annual respiratory epidemics and the threat of pandemic infections. The effect of the materials in this virus was analyzed in Fig. 7C. In contact with the G3 material, viral burden was reduced around 100,000 times as compared to the control or the G1 material. In the case of the kaolin materials, the one containing Ag nanoparticles was able to reduce 1000 times the viable virus remaining in the supernatant, while the one containing CuO nanoparticles was similar in activity to the G3, reducing between 10,000 and 100,000 times the amount of influenza virus remaining in the supernatant.

SARS-CoV-2 was also included in the study as the virus that has presented the highest social impact in the human population worldwide, causing COVID-19. The effect of the materials in this virus was analyzed in Fig. 7D. As expected, the effect of the materials on this virus was similar to the one observed against the enveloped HSV-1 and influenza viruses. In this case, G1 was able to reduce the virus present in the supernatant around 100 times, while the G3 was able to reduce the virus present in the supernatant between 10,000 and 100,000 times. Kaolin-based materials had an effect inducing a reduction of SARS-CoV-2 in the supernatant under detectable levels. Exact values for means and ±SD values are listed in Supplementary Table 6.

4. Discussion

Current SARS-CoV-2 pandemic raises the need for developing materials to remove human or animal infectious agents from surfaces, waters, or air. Viral pandemic or outbreak scenarios will demand materials that could be adapted to different situations. This work presents two kinds of low-cost inorganic materials, i.e., glass-based, and kaolin-based materials, that could be adapted to different situations to prevent or reduce the presence of infectious circulating viruses.

In parallel, the use of protective equipment with viral disabling characteristics, is an interesting strategy to prevent infections. Exposure to the virus during several labor hours increases the chances of infection and requires a better effort to improve materials that can improve personal safety. The use of liquid disinfectants in cleaning surfaces may present several problems such as the need to repetitive cleaning or difficulties in reaching certain areas or treating specific surfaces.

Virus (and other infectious agents) inactivation can be achieved by physical and chemical methods. Several mechanisms have been proposed for virus inactivation like oxidation of viral surfaces or altering viral attachment and fusion events [34]. Alteration of the genetic material is another possible mechanism that can be achieved through nucleic acid breaking or crosslinking [35]. Finally, alteration of viral membranes or naked capsids can be an alternative strategy to destroy viruses [36].

To date there are no reports in the literature about a glass/bioglass with the forceful virucidal activity shown by the G3 glass (Figs. 1 and 7). This glass can be considered a low-cost material that can be fabricated in thousands of tons following a conventional industrial process. Furthermore, G3 material has interesting properties due to its stability and low toxicity. The mechanism behind its antiviral activity seems to induce virus aggregation as observed in Fig. 6F. This property is not solely associated to a virus adsorption as observed in Fig. 4, since the amount of proteins in the supernatants containing viruses in contact with G3 is comparable to G1 control or the original virus preparation (Fig. 6). The behavior of this glass or the corresponding elements present in the lixiviate in contact with the viruses, must be sought, not only in the depolarization effect of membranes, which has already been widely proven in bacteria (resistant and not resistant to antibiotics such as MRSA) and yeasts [29] and now against viruses.

We consider that the broad spectrum that G3 shows against different microorganisms such as bacteria, yeasts and particularly against viruses may be related to the synergistic effect of the joint leaching of calcium and boron ions. Similar effects have been found in the literature, i.e. in the case of joint Ag^{+} and Ca^{2+} leachates against yeasts, which increases the very low biocidal activity of silver by more than 3 orders of magnitude [37]. In the case of Ca^{2+} and B^{3+}, more research will be required in the future to elucidate what type of mechanism is acting.

Kaolin-based materials have a different mode to interact with viruses. In comparison with G3, these materials can retain the virus in their surface. G3 has a specific surface area of less than 1 m^2/g, while that of kaolin is of the order of 15 m^2/g. Kaolin surfaces are long known for having virus adsorption properties [38]. However, ζ-potential analysis of materials in contact with the virus (Supplementary Table 5) presents a possible interaction with both glass and kaolin-based materials. Further characterization of the physical interaction between viruses and the materials will be required. Hydrophilic characteristics in kaolin can favor viral adsorption, trapping the virus and inducing structural distortion of virion proteins and thus blocking viral entry into cells[39]. This property however is not universal for all kind of viruses. In our case, both adenovirus (Fig. 7A) and influenza virus (Fig. 7C) seem to scape to this physical property of kaolin, at least on the experimental conditions used in our assays. Viral adsorption may depend on variables like pH, isoelectric point of the viral proteins, or protein hydration. These factors have been described to influence kaolin adsorption[40]. It is also totally harmless to humans, as compared to metallic nanoparticles as well as environmentally friendly.

Kaolin-based materials can be modified, and, in our case, these modifications are pivotal to introduce an enhanced antiviral effect. Introduction of CuO and Ag nanoparticles associated to the kaolin increases the ability of the material to inactivate viruses. These metal-based nanoparticles can be detached from the constitutional kaolinite plates and have antiviral activity on their own, as observed inFig. 4. That is, the kaolinite plates act as a dispenser for the metallic nanoparticles, allowing only the required fraction to be supplied to the medium for the elimination of viruses. After 24 h that the kaolin-based materials were in contact with the media, only a 0.1% of the total silver and a 2% of the total copper were released to the media (Fig. 5C). The rest of the nanoparticles would remain adhered to the surface of the kaolinite plates, avoiding their discharge into the environment.

In any case, it seems that in the kaolin series, virus infectivity could be affected by release of active elements in lixiviates (Figs. 4 and 5) as well as adsorption and inactivation. The additional properties of the metals may enhance the ability of the material to trap and disable the virus. Future experiments will determine how CuO and Ag nanoparticles may affect virus infectivity in the materials under study.

CuO-based nanoparticles are long known for having antimicrobial properties, including viruses[41,42]. Although the material containing CuO has some cell toxicity (Fig. 3), applications of this material containing Cu could be adapted to situations where this toxicity is not an issue. In comparison to CuO, Ag-based kaolin has also a broad antiviral activity against all the viruses tested (Figs. 2 and 7). This antiviral activity is not as powerful as the one comingfrom the CuO material, however the toxicity of the material containing Ag (Fig. 3) is also lower that the one with CuO and this could be of interest as well. Lower activity could be attributed also to the lower percentage of Ag (2%) vs. Cu (5%) in the corresponding materials, or just justified by the differences in Ag and Cu as well as their corresponding oxidation states. Available studies on the toxicity of silver nanoparticles are sometimes contradictory [43]. Induction of toxicity fluctuates with different concentrations of silver nanoparticles in different cell lines. Nanoparticle properties (i.e, size, shape, concentration, surface properties, agglomeration, or aggregation), cell line and exposure time play vital roles in cytotoxicity. The minimum or highest concentration of silver nanoparticles needed to induce toxicity is not fixed and might vary based on the organism[44]. Something similar happens with copper oxide nanoparticles[45].

Manipulation of nanoparticles of CuO/Ag has challenging issues, since they need expensive chemical processes that would limit its application to very specific cases, limiting the large-scale production. Here we show the viability in manipulating them supporting the nanoparticles in an inorganic vehicle such as kaolin is a way to overcome this limitation and to avoid the problems of nanoparticles' agglomeration. On the other hand, kaolinite is largely considered as a clay mineral with an extraordinary rheological behavior[46]. This fact will facilitate the homogeneous distribution of these Ag/CuO nanoparticles in stable suspensions (impossible to achieve with individual metal/metal oxide nanoparticles) for their subsequent application either as paints or atomized to be applied in open and/or closed spaces that require decontamination.

The results obtained in this investigation provide proof-of-principle and encourage further developments.Initial attempts to develop prototype surfaces containing these active virucidal materials (glasses and nanoparticles supported on kaolin) are currently undergoing. The challenge to maintain the particle size and the surface in contact with the virus is an important aspect that must be solved in future steps. Further incorporation of materials into filters, resins or immobilized matrixes could also be addressed to implement the use of these materials in air or liquid cleaning systems.

5. Conclusions

Low-cost inorganic particulate systems [i.e., a glass (G3), and supported metallic/metal oxide nanoparticles on kaolin (K-nAg/nCu)] showed strong antiviral properties (a reduction of viral infectivity higher than 99.9% in 1 h of contact) against model viruses such as encapsidated viruses like (adenovirus) or enveloped viruses such as vesicular stomatitis virus, influenza virus, pandemic SARS-CoV-2 as well as herpes simplex virus type I (HSV-1). The mechanism behinds their antiviral activity is related with the properties of the materials, that suggests virus aggregation in the case of G3 glass or adsorption in the case of kaolin-based materials, but also with the nanoparticles and ions released from them. Additionally, it has been proved that the kaolinite plates act as a dispenser for the metallic nanoparticles, allowing only the required fraction to be supplied to the medium for the elimination of viruses. The rest of the nanoparticles would remain attached to the surface of the kaolinite plates, avoiding their transfer to the environment.

Funding

This research was performed with support from The Spanish National Research Council (CSIC) (Project No 202060E109). M.F. is grateful to the Comunidad Autonoma de Madrid for research project No. 2017-T1/BIO-4992 (“Atracción de Talento” Action) cofunded by Universidad Complutense de Madrid. This publication was also supported by the European Virus Archive GLOBAL (EVA-GLOBAL) project that has received funding from the European Union's Horizon 2020 research and innovation program under grant agreement 871029. S. R.-R. was supported by the the FPI fellowship funded by Universidad San Pablo CEU. J.A-H. was supported by the PFIS fellowship co-funded by the FEDER/FSE and the ISCIII.

Credit author statement

Conceptualization. José S Moya, Belen Cabal, Estanislao Nistal-Villan. Methodology. Sergio Rius-Rocabert, Javier Arranz-Herrero, Adolfo Fernández-Valdés, Marzia Marciello, Sandra Moreno, Francisco Llinares-Pinel, Jesus Presa, Antonia García, Alejandro Brun, Marco Filice, José S Moya, Belen Cabal, Estanislao Nistal-Villan. Software. Jesus Presa, Validation. Sergio Rius-Rocabert, Adolfo Fernández-Valdés, Belen Cabal, Estanislao Nistal-Villan. Investigation. Sergio Rius-Rocabert, Javier Arranz-Herrero, Adolfo Fernández-Valdés, Marzia Marciello, Sandra Moreno, Francisco Llinares-Pinel, Jesus Presa, Antonia García, Alejandro Brun, Marco Filice, José S Moya, Belen Cabal, Estanislao Nistal-Villan. Resources. Alejandro Brun, Rubén Hernández, Marco Filice, José S Moya, Belen Cabal, Estanislao Nistal-Villan. Writing - Original Draft. Sergio Rius-Rocabert, Javier Arranz-Herrero, Adolfo Fernández-Valdés, Belen Cabal, Estanislao Nistal-Villan. Writing - Review & Editing. Sergio Rius-Rocabert, Javier Arranz-Herrero, Adolfo Fernández-Valdés, Marzia Marciello, Sandra Moreno, Francisco Llinares-Pinel, Jesus Presa, Rubén Hernandez-Alcoceba, Roberto López-Píriz, Ramón Torrecillas, Antonia García, Alejandro Brun, Marco Filice, José S Moya, Belen Cabal, Estanislao Nistal-Villan. Visualization. Sergio Rius-Rocabert, Javier Arranz-Herrero, Adolfo Fernández-Valdés, Jesús Presa, Belen Cabal, Estanislao Nistal-Villan. Supervision. Belen Cabal, Estanislao Nistal-Villan. Project administration. Belen Cabal, Estanislao Nistal-Villan. Funding acquisition. Belen Cabal.

Declaration of competing interest

The authors declare that they have no known competing financial interests or personal relationships that could have appeared to influence the work reported in this paper.

Acknowledgements

In memoriam: Prof. Antonio Carlos da Silva passed away on April 3, 2021 from COVID-19 complications. He actively participated in the initial development of G3 glass. His premature death is an immeasurable loss.

Appendix A. Supplementary data

Supplementary data to this article can be found online at https://doi.org/10.1016/j.mtbio.2021.100191.

References

[1] Z. Tang, et al., A materials-science perspective on tackling COVID-19, Nat. Rev. Mater. (2020) 1–14.
[2] N. van Doremalen, et al., Aerosol and surface stability of SARS-CoV-2 as compared with SARS-CoV-1, N. Engl. J. Med. 382 (16) (2020) 1564–1567.
[3] J. Biryukov, et al., Increasing temperature and relative humidity accelerates inactivation of SARS-CoV-2 on surfaces, mSphere (4) (2020) 5.
[4] S. Riddell, et al., The effect of temperature on persistence of SARS-CoV-2 on common surfaces, Virol. J. 17 (1) (2020) 145.
[5] M.K. Ijaz, et al., Microbicidal actives with virucidal efficacy against SARS-CoV-2 and other beta- and alpha-coronaviruses and implications for future emerging coronaviruses and other enveloped viruses, Sci. Rep. 11 (1) (2021) 5626.
[6] T. Labadie, et al., Historical discoveries on viruses in the environment and their impact on public health, Intervirology 63 (1–6) (2020) 17–32.
[7] T.R. Julian, J.O. Leckie, A.B. Boehm, Virus transfer between fingerpads and fomites, J. Appl. Microbiol. 109 (6) (2010) 1868–1874.
[8] E.A. Varughese, et al., Estimating virus occurrence using Bayesian modeling in multiple drinking water systems of the United States, Sci. Total Environ. (2018) 1330–1339, 619-620.
[9] V. Stadnytskyi, et al., The airborne lifetime of small speech droplets and their potential importance in SARS-CoV-2 transmission, Proc. Natl. Acad. Sci. U. S. A. 117 (22) (2020) 11875–11877.
[10] N. Castano, et al., *Fomite transmission, physicochemical Origin of virus-surface interactions, and disinfection Strategies for enveloped Viruses with Applications to SARS-CoV-2.* ACS omega 6 (10) (2021) 6509–6527.
[11] S. Talebian, et al., Nanotechnology-based disinfectants and sensors for SARS-CoV-2, Nat. Nanotechnol. 15 (8) (2020) 618–621.
[12] S. Galdiero, et al., Silver nanoparticles as potential antiviral agents, Molecules 16 (10) (2011) 8894–8918.
[13] C. Das, et al., Silver-based Nanomaterials as therapeutic agents against coronaviruses: a review, Int. J. Nanomed. 15 (2020) 9301–9315.
[14] D. Bennet, et al., Evaluation of supercritical CO(2) sterilization efficacy for sanitizing personal protective equipment from the coronavirus SARS-CoV-2, Sci. Total Environ. 780 (2021) 146519.
[15] E. Mantlo, et al., In vitro efficacy of a copper iodine complex PPE disinfectant for SARS-CoV-2 inactivation, F1000Res 9 (2020) 674.
[16] X. Hang, et al., Antiviral activity of cuprous oxide nanoparticles against Hepatitis C Virus in vitro, J. Virol. Methods 222 (2015) 150–157.
[17] M. Rai, et al., Metal nanoparticles: the protective nanoshield against virus infection, Crit. Rev. Microbiol. 42 (1) (2016) 46–56.

[18] S. Riela Giuseppe, R.F. Fakhrullin, *Clay-based drug-delivery systems: what does the future hold?* Ther Deliv 8 (8) (2017) 633–646.
[19] G. Choi, et al., Vectorized clay nanoparticles in therapy and diagnosis, Clay Clay Miner. 67 (1) (2019) 25–43.
[20] N. Khatoon, M.Q. Chu, C.H. Zhou, Nanoclay-based drug delivery systems and their therapeutic potentials, J. Mater. Chem. B 8 (33) (2020) 7335–7351.
[21] R. de Melo Barbosa, et al., 8-Nanoclays in drug delivery systems, in: G. Cavallaro, R. Fakhrullin, P. Pasbakhsh (Eds.), Clay Nanoparticles, Elsevier, 2020, pp. 185–202.
[22] B. Cabal, et al., Heterogeneous precipitation of silver nanoparticles on kaolinite plates, Nanotechnology 21 (47) (2010) 475705.
[23] M. Massaro, et al., The use of some clay minerals as natural resources for drug carrier applications, J. Funct. Biomater. (4) (2018) 9.
[24] L.Y. Ozer, et al., Water microbial disinfection via supported nAg/Kaolin in a fixed-bed reactor configuration, Appl. Clay Sci. 184 (2020) 105387.
[25] L. Drago, et al., Antimicrobial activity and resistance selection of different bioglass S53P4 formulations against multidrug resistant strains, Future Microbiol. 10 (8) (2015) 1293–1299.
[26] J.S. Moya, et al., Mechanism of calcium lixiviation in soda-lime glasses with a strong biocide activity, Mater. Lett. 70 (2012) 113–115.
[27] B. Cabal, et al., A new biocompatible and antibacterial phosphate free glass-ceramic for medical applications, Sci. Rep. 4 (2014) 5440.
[28] M. Bortolin, et al., Antibiofilm agents against MDR bacterial strains: is bioactive glass BAG-S53P4 also effective? J. Antimicrob. Chemother. 71 (1) (2016) 123–127.
[29] J.S. Moya, et al., Glass powders with a high content of calcium oxide: a step towards a "green" universal biocide, Adv. Eng. Mater. (6) (2011) 13, p. B256-B260.
[30] E. Santamaría, et al., Identification of replication-competent HSV-1 Cgal+ strain targets in a mouse model of human hepatocarcinoma xenograft, J. Proteonomics 73 (1) (2009) 153–160.
[31] E. Nistal-Villan, et al., Negative role of RIG-I serine 8 phosphorylation in the regulation of interferon-beta production, J. Biol. Chem. 285 (26) (2010) 20252–20261.
[32] E. Nistal-Villan, et al., Enhanced therapeutic effect using sequential administration of antigenically distinct oncolytic viruses expressing oncostatin M in a Syrian hamster orthotopic pancreatic cancer model, Mol. Cancer 14 (2015) 210.
[33] L.J. Reed, H. Muench, A simple method of estimating fifty per cent endpoints12, Am. J. Epidemiol. 27 (3) (1938) 493–497.
[34] A. Habibi-Yangjeh, et al., Review on heterogeneous photocatalytic disinfection of waterborne, airborne, and foodborne viruses: can we win against pathogenic viruses? J. Colloid Interface Sci. 580 (2020) 503–514.
[35] G. McDonnell, A.D. Russell, Antiseptics and disinfectants: activity, action, and resistance, Clin. Microbiol. Rev. 12 (1) (1999) 147–179.
[36] J. Torrey, U. von Gunten, T. Kohn, Differences in viral disinfection mechanisms as revealed by quantitative transfection of echovirus 11 genomes, Appl. Environ. Microbiol. (14) (2019) 85.
[37] L. Esteban-Tejeda, et al., The antibacterial and antifungal activity of a soda-lime glass containing silver nanoparticles, 085103, Nanotechnology 20 (8) (2009).
[38] K.J. Clark, et al., In vitro studies on the use of clay, clay minerals and charcoal to adsorb bovine rotavirus and bovine coronavirus, Vet. Microbiol. 63 (2–4) (1998) 137–146.
[39] M.E. Awad, et al., Modeling of the adsorption of a protein-fragment on kaolinite with potential antiviral activity, Appl. Clay Sci. 199 (2020) 105865.
[40] C.P. Gerba, Applied and theoretical aspects of virus adsorption to surfaces, Adv. Appl. Microbiol. 30 (1984) 133–168.
[41] G. Tortella, et al., Bactericidal and virucidal activities of biogenic metal-based nanoparticles: advances and perspectives, Antibiotics (7) (2021) 10. Basel.
[42] P. Merkl, et al., Antiviral activity of silver, copper oxide and zinc oxide nanoparticle coatings against SARS-CoV-2, Nanomaterials (5) (2021) 11. Basel.
[43] F. Pilaquinga, et al., Silver nanoparticles as a potential treatment against SARS-CoV-2: a review, e1707, Wiley Interdiscip. Rev. Nanomed. Nanobiotechnol. (5) (2021) 13.
[44] M. Akter, et al., A systematic review on silver nanoparticles-induced cytotoxicity: Physicochemical properties and perspectives, J. Adv. Res. 9 (2018) 1–16.
[45] S. Naz, A. Gul, M. Zia, Toxicity of copper oxide nanoparticles: a review study, IET Nanobiotechnol. 14 (1) (2020) 1–13.
[46] W.D. Kingery, H.K. Bowen, R. Uhlmann Donald, Introduction to Ceramics, second ed., John Wiley & Sons, , New York, 1976, p. 1056, ed. W.S.o.t.S.a.T.o. Materials.